Editors' Suggestion

New Regime of Inertial Alfvén Wave Turbulence in the Auroral Ionosphere

Francesca Di Mare[1,2,*] and Gregory G. Howes[3]
[1]NASA Goddard Space Flight Center, Greenbelt, Maryland, USA
[2]The Catholic University of America, Washington, DC, USA
[3]Department of Physics and Astronomy, University of Iowa, Iowa City, Iowa, USA

(Received 22 January 2024; accepted 4 June 2024; published 22 July 2024)

We investigate a new regime of inertial Alfvén wave turbulence observed in the very low beta plasma of the auroral ionosphere using electric and magnetic field measurements by the TRICE-2 sounding rocket. Combining the observed features of the electric and magnetic field frequency spectra with the linear properties of inertial Alfvén waves, we deduce the path of the anisotropic turbulent cascade through wave vector space. We find a critically balanced cascade through the magnetohydrodynamic scales of the inertial range down to the perpendicular scale of the plasma skin depth, followed by a parallel cascade to the ion inertial length. We infer damping of the cascade by a combination of proton cyclotron damping and electron Landau damping.

DOI: 10.1103/PhysRevLett.133.045201

Introduction—Plasma turbulence plays an important role in governing the transport of mass, momentum, and energy in space plasmas throughout the heliosphere, from the solar corona to the solar wind to the planetary magnetospheres. At the Earth, turbulence [1] and Alfvén waves [2,3] play a key role in magnetosphere-ionosphere coupling, where kinetic energy is deposited in the ionosphere through the precipitation of energetic particles [4], leading to fascinating space plasma phenomena, such as the glowing of the aurora. The auroral regions at high latitude are associated with the polar cusp and the plasma sheet boundary layer, with precipitating electrons arising from the dayside magnetospheric boundary layer [5] or the nightside plasma sheet [6]. These electrons are accelerated into the loss cone by quasistatic field-aligned currents [7,8] or Earthward propagating Alfvén waves [2,3].

Under the very low plasma beta conditions of the auroral magnetosphere probed by the TRICE-2 rocket mission, with $\beta_p < m_e/m_p$, Alfvén waves with perpendicular scales smaller than the plasma skin depth, $k_\perp d_e \gtrsim 1$, become dispersive, with a decreasing phase velocity as $k_\perp$ increases due to electron inertia—such Alfvénic wave modes in this limit are denoted "inertial Alfvén waves" [9]. Unlike Alfvén waves in the magnetohydrodynamic (MHD) limit $k_\perp d_e < 1$, the electric field of inertial Alfvén waves develops a parallel component due to the electron inertia [10]. With the very low beta plasma parameters yielding an Alfvén velocity faster than the electron thermal velocity $v_A > v_{te}$, these waves have been proposed to accelerate electrons with energies of a few eV, within the suprathermal tail of the electron velocity distribution, up to the keV energies associated with precipitating auroral electrons associated with small-scale dynamic aurora [2,3,11,12]. Coordinated spacecraft observations of Alfvén wave energy fluxes at high altitudes and precipitating electrons at lower altitudes provide strong evidence for this electron acceleration mechanism [13–17] and recent laboratory experiments confirmed that inertial Alfvén waves do accelerate electrons under auroral conditions [18–20]. Measurements from the *Freja* spacecraft also found broadband turbulence consisting of dispersive Alfvén waves on field lines within the auroral oval [1].

Here, we explore this new regime of inertial Alfvén wave turbulence in the auroral magnetosphere through a detailed analysis of the turbulent electric and magnetic field frequency spectra. Combining the linear properties of the inertial Alfvén wave mode with the observed features of the turbulence enables us to deduce the number density ratio of hydrogen to oxygen ions in the multi-ion ionospheric plasma, to estimate the path of the turbulent energy cascade to small scales in wave vector space, and to predict the kinetic damping mechanisms that likely govern the dissipation of the turbulence.

Observations—The Twin Rockets to Investigate Cusp Electrodynamics-2 (TRICE-2) flew from Norway's Andøya Space Center on December 8, 2018, through the Earth's Cusp region. Part of NASA's Grand Challenge Initiative CUSP Project, the mission launched a pair of almost identically instrumented scientific payloads at 08:26 UT and 08:28 UT respectively, along very similar ground

*Contact author: francesca.dimare@nasa.gov

tracks: the High Flyer 52.003 (HF03) reached a maximum altitude of 1042 km and the Low Flyer 52.004 (LF04) reached a maximum altitude of 756 km. Both rockets carried sophisticated, high frequency instruments including three-axis flux-gate magnetometers and electric field sensors oriented perpendicular to the rocket spin axes, with a sampling rate of 2.5 kHz. The background conditions of the interplanetary magnetic field prior to launch had a steady negative $B_z \sim 5$ nT component and evidence of ionospheric signatures of reconnection such as poleward-moving auroral forms confirmed by ground optical and radar data [21]. Both payloads traversed an active polar cusp, with enhanced electron densities and increases in the occurrence and intensity of plasma waves seen by the very low frequency and high frequency receivers, also encountering particle fluxes precipitating down the magnetic field lines [22].

Because of its cleaner entrance into the cusp when compared to the LF04 [23], we analyze the HF03 flyer observations near apogee over 700 s $\leq t \leq$ 750 s, an interval with relatively steady background plasma parameters. Interval-averaged plasma parameters include the magnetic field $B = 3.7 \times 10^{-5}$ T, electron density $n_e = 2.8 \times 10^9$ m^{-3}, and rocket velocity $v_r = 2.0$ km/s at an angle $\theta_{Bv} = 63°$ from the mean magnetic field. Concurrent EISCAT radar observations [24] at 600 km altitude are used to estimate the ion and electron temperatures, $T_i \simeq 0.2$ eV and $T_e \simeq 0.34$ eV. These parameters yield an Alfvén velocity (assuming a proton-only plasma) of $v_A = B/(\mu_0 n_i m_i)^{1/2} = 15000$ km/s and an electron thermal velocity of $v_{te} = (2T_e/m_e)^{1/2} = 350$ km/s, satisfying the inertial regime condition $v_A > v_{te}$. Cyclotron frequencies for hydrogen and singly charged oxygen are $f_{cp} = 560$ Hz and $f_{cO^+} = 35$ Hz. The fundamental dimensionless parameters for the observed interval are the proton beta plasma $\beta_p = 1.7 \times 10^{-7}$, proton-to-electron temperature ratio $T_p/T_e = 0.6$, and $v_{tp}/c = 2 \times 10^{-5}$. In the inertial Alfvén wave regime, perpendicular length scales are normalized by the plasma skin depth $d_e = c/\omega_{pe} = 0.10$ km and parallel length scales are normalized by the proton inertial length $d_p = c/\omega_{pp} = v_A/\Omega_p = 4.3$ km.

The electric and magnetic field measurements are Lorentz transformed from the rocket frame (primed) to the plasma rest frame (unprimed) using $\boldsymbol{E} = \boldsymbol{E}' - \boldsymbol{v_r} \times \boldsymbol{B}'$ and $\boldsymbol{B} = \boldsymbol{B}'$ for the nonrelativistic limit $v_r/c \ll 1$ [25]. This procedure is essential in the limit that the probe velocity is much larger than the Alfvén velocity, $v_r \gg v_A$, to eliminate the electric field arising from the convection of the magnetic field past the probe [26]; the TRICE-2 rocket measurements are in the opposite limit $v_r \ll v_A$, so, other than the nearly constant convection electric field associated with the Earth's equilibrium dipole magnetic field, this transform has a negligible effect on the measured turbulent electric field fluctuations, but we perform the Lorentz transformation nonetheless.

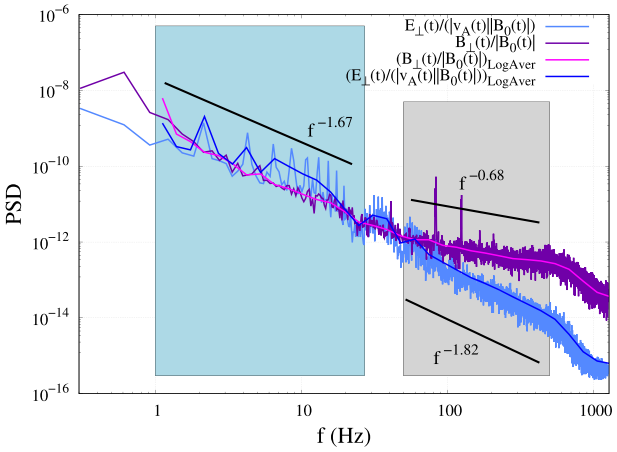

FIG. 1. Normalized perpendicular magnetic $B_\perp(t)/|B_0(t)|$ and electric field $E_\perp(t)/(|v_A(t)||B_0(t)|)$ frequency spectra from the TRICE-2 high flyer over 700–750 s. We interpreted two frequency ranges: the MHD Alfvén wave regime at $k_\perp d_e < 1$ (blue shading) and the dispersive inertial Alfvén regime (gray shading).

The local mean magnetic field $\mathbf{B}_0(t)$ is determined by a boxcar average over the ~2 s rocket spin period, with an interval-averaged $\langle \mathbf{B}_0(t) \rangle = (1.83 \times 10^{-7}, 4.57 \times 10^{-6}, -3.63 \times 10^{-5})$ T in (E, N, U) coordinates. We use the boxcar-averaged $\mathbf{B}_0(t)$ to rotate the $\mathbf{E}(t)$ and $\mathbf{B}(t)$ measurements into a magnetic field-aligned coordinate (FAC) system $(\hat{\mathbf{e}}_{\perp 1}, \hat{\mathbf{e}}_{\perp 2}, \hat{\mathbf{b}})$. The orthonormal unit vectors of the FAC system are defined at each time by $\hat{\mathbf{b}}(t) = \mathbf{B}_0(t)/|\mathbf{B}_0(t)|$, $\hat{\mathbf{e}}_{\perp 2}(t) \propto \hat{\mathbf{b}}(t) \times \hat{\mathbf{e}}_E$, and $\hat{\mathbf{e}}_{\perp 1}(t) \propto \hat{\mathbf{e}}_{\perp 2}(t) \times \hat{\mathbf{b}}(t)$, where $\hat{\mathbf{e}}_E$ is the East unit vector. Projecting the electric and magnetic fields onto the FAC system at each time yields the perpendicular components of both fields as a function of time.

Finally, we Fourier transform in time the normalized perpendicular components $E_\perp(t)/[v_A(t)B_0(t)]$ and $B_\perp(t)/B_0(t)$ and plot the frequency spectra logarithmically in Fig. 1, showing full-resolution electric (light blue) and magnetic (purple) field spectra along with logarithmically averaged electric (blue) and magnetic (magenta) field spectra to visualize more clearly the spectral slopes. The full-resolution electric field (light blue) is contaminated by 2 Hz spin tones and its harmonics, so we interpret the true, uncontaminated spectrum to coincide with the low values between the spikes. The frequency spectra show two breaks at $f_{b1} \sim 50$ Hz and $f_{b2} \sim 500$ Hz. With this normalization of the fields, the electric and magnetic field frequency spectra are generally coincident at $f < 50$ Hz (blue shading), with the electric field spectrum steepening and the magnetic field spectrum flattening up to the second break over the range 50 Hz $< f <$ 500 Hz (gray shading). By comparison, spacecraft measurements [27] and kinetic numerical simulations [28–32] of turbulence in the kinetic regime ($\beta_p > m_e/m_p$, the opposite limit of the inertial

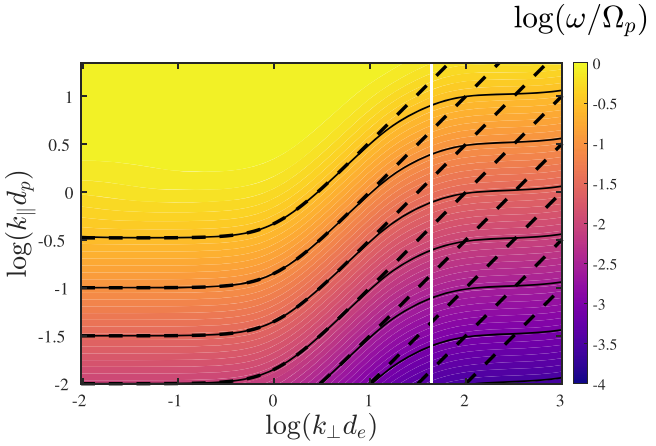

FIG. 2. A comparison of the normalized frequency ω/Ω_p of the inertial Alfvén wave over the normalized wave vector plane $(k_\perp d_e, k_\parallel d_p)$ (color map and solid contours) to the analytical approximation (1) (dashed contours), with the $k_\perp d_e = v_A/v_{te}$ limit plotted (white vertical line).

regime [9]) observe the opposite trend at high frequencies: a steepening of the magnetic field spectrum and a flattening of the electric field spectrum, attributed to the linear physics of kinetic Alfvén waves [27–29]. Below we explain the properties of this new regime of inertial Alfvén wave turbulence in the auroral ionosphere in terms of the kinetic plasma physics of linear waves.

Analysis—Even in the presence of strong plasma turbulence—in which the timescale of the nonlinear energy transfer to smaller scales balances with the linear wave period at that scale, a condition known as critical balance [33]—the small amplitude of the turbulent fluctuations $|\delta\mathbf{B}|/|\mathbf{B}| \ll 1$ implies that we expect those fluctuations to be consistent with the eigenfunctions of the linear wave modes of the plasma [28,29,34–38]. In the very low proton plasma beta limit $\beta_p \ll m_e/m_p$ relevant for these observations, the linear dispersion relation of inertial Alfvén waves is well approximated by [39]

$$\frac{\omega}{\Omega_p} = \frac{k_\parallel d_p}{\sqrt{1 + (k_\perp d_e)^2 + (k_\parallel d_p)^2}}. \tag{1}$$

In Fig. 2, we plot the normalized frequency ω/Ω_p (color map and solid contours) of the Vlasov-Maxwell dispersion relation using the PLUME solver [40] for isotropic Maxwellian proton and electron equilibrium velocity distributions with parameters $\beta_p = 1.7 \times 10^{-7}$, $T_p/T_e = 0.6$, and $v_{tp}/c = 2 \times 10^{-5}$ compared to the solutions for (1) (dashed contours). The analytical form is accurate in the limits $k_\parallel d_p < 1$ and $k_\perp d_e < v_A/v_{te}$ (white vertical line), where the deviation at $k_\perp d_e \gtrsim v_A/v_{te}$ occurs because the phase velocity of the inertial Alfvén wave drops to the electron thermal velocity, $\omega/(k_\parallel v_{te}) \to 1$, leading to strong electron Landau damping.

In the MHD limit, turbulence typically generates an anisotropic cascade with $k_\parallel/k_\perp \ll 1$ at sufficiently small scales [33,41–45]. For such small scale, anisotropic fluctuations in the low plasma beta $\beta_p \ll 1$ limit relevant here, the MHD Alfvén wave frequency is well separated from the fast and slow magnetosonic modes, with $\omega_A/\omega_F \sim k_\parallel/k_\perp \ll 1$ and $\omega_A/\omega_S \sim \beta_p^{-1/2} \gg 1$. These disparate timescales suggests weak nonlinear interactions between the magnetosonic and Alfvénic modes, so we expect the Alfvénic modes (and their kinetic extension) will dominate the properties of the observed turbulent fluctuations.

A fundamental difference between spacecraft measurements of turbulence in the solar wind and the TRICE-2 rocket measurements is that the ionospheric plasma contains multiple ion species, with the ion species at the TRICE-2 high flyer apogee of $z \sim 1000$ km predicted to be a mixture of predominantly hydrogen H^+ and singly charged oxygen O^+ [46], characterized by the number density ratio n_O/n_p. In this two-ion plasma, the Alfvén velocity may be expressed as $v_{A(p,O)} = v_A/[1+(n_O/n_p)(m_O/m_p)]^{1/2}$, where the proton-only Alfvén velocity is defined by $v_A \equiv B/(\mu_0 n_p m_p)^{1/2}$. In Fig. 1, the normalized magnetic and electric field frequency spectra at $f < 50$ Hz (blue shading) are generally coincident, with the electric field steepening and the magnetic field flattening at higher frequencies 50 Hz $< f <$ 500 Hz (gray shading). If we assume that (i) the first break at $f_{b1} \simeq$ 50 Hz represents the transition from the MHD to the kinetic regime $k_\perp d_e \sim 1$ and (ii) the turbulent fluctuations are dominated by incompressible Alfvénic fluctuations, we may use the observed perpendicular magnetic and electric field frequency spectra at $f < f_{b1}$ and Faraday's Law to determine the ion composition of the plasma.

In the MHD limit $k_\perp d_e < 1$, for an Alfvén wave polarized in the y direction with $\mathbf{k} = k_\perp \hat{\mathbf{x}} + k_\parallel \hat{\mathbf{z}}$, the Fourier-transformed y component of Faraday's Law can be expressed as $\omega(\mathbf{k})/k_\parallel \simeq \hat{E}_x(\mathbf{k})/\hat{B}_y(\mathbf{k})$; this result exploits the fact that $\hat{E}_z(\mathbf{k}) \ll \hat{E}_x(\mathbf{k})(k_\parallel/k_\perp)$, a limit verified by the PLUME solver [40]. For Alfvén waves polarized in both of the directions perpendicular to $\mathbf{B}$, and substituting the MHD Alfvén wave linear dispersion relation $\omega = \pm k_\parallel v_A$, we expect a turbulent spectrum of Alfvénic fluctuations to satisfy $E_\perp/(v_A B_\perp) \sim \pm 1$. The normalized energy spectra at $f < 50$ Hz in Fig. 1 satisfy this expectation using the proton-only Alfvén velocity v_A, suggesting an upper limit on the oxygen-to-proton number density ratio $n_O/n_p \lesssim m_p/m_O = 1/16$, providing a novel means of observationally constraining the number density ratio in a turbulent, two-ion plasma.

To assess whether a minority fraction $n_O/n_p \lesssim 1/16$ would impact the turbulent dynamics, in Fig. 3 we plot the Alfvén wave (a) frequency ω/Ω_p and (b) damping rate $-\gamma/\omega$ vs $k_\parallel d_p$ from PLUME with the same parameters as Fig. 2 but with $T_O/T_p = 1$ and density ratios n_O/n_p of 0

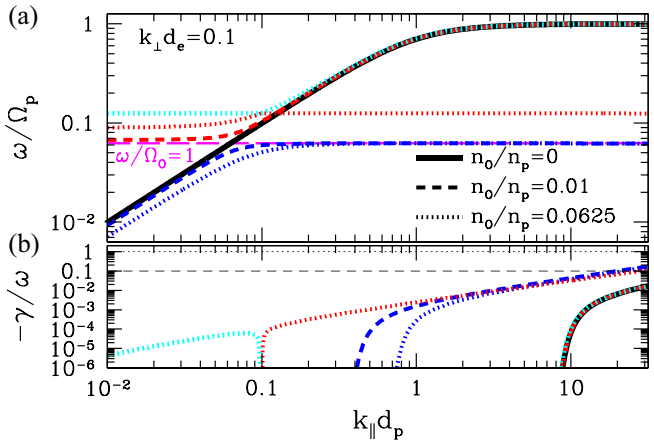

FIG. 3. The Alfvén wave (a) frequency ω/Ω_p and (b) damping rate $-\gamma/\omega$ vs $k_\parallel d_p$ for $k_\perp d_e = 0.1$ for a two-ion plasma with n_O/n_p of 0 (solid), 0.01 (dashed), and 1/16 (dotted).

(thick black solid), 0.01 (dashed), and 1/16 (dotted). Although the oxygen cyclotron resonance $\omega/\Omega_O = 1$ (magenta long dashed) leads to a small frequency gap for $n_O/n_p = 0.01$, and a slightly larger gap for $n_O/n_p = 1/16$, the propagating parts of the wave solutions (regions with nonzero slope $\partial\omega/\partial k_\parallel$) approximately reproduce the Alfvén wave dispersion relation with $n_O/n_p = 0$. For $n_O/n_p = 1/16$, there is also an oxygen Bernstein wave mode conversion [34] at $\omega/\Omega_O = 2$ (red to cyan dotted). Even with these small gaps and mode conversions, the nonlinear Alfvén wave interactions mediating the turbulent cascade [45] can transfer energy along the Alfvén wave dispersion relation across these narrow features in frequency, although the presence of the oxygen cyclotron wave at $\omega/\Omega_O = 1$ may lead to the bumps in the energy spectra observed at $f \sim f_{cO^+} = 35$ Hz in Fig. 1. Furthermore, the small damping rates $-\gamma/\omega \ll 1$ in Fig. 2(b) imply negligible damping of the turbulent fluctuations at the transition through $\omega/\Omega_O = 1$. This evidence suggests the lowest-order turbulent dynamics will remain unchanged relative to the Alfvén wave properties of the proton-only plasma in Fig. 2.

The frequency of turbulent fluctuations in the rocket frame of reference ω_r is given by the sum of the plasma-frame frequency ω and the frequency of Doppler-shifted spatial structure, $\omega_r = \omega + \mathbf{k}\cdot\mathbf{v}_r$ [25], where $\mathbf{v}_r$ is the rocket velocity relative to the plasma and $\mathbf{k}$ is the 3D wave vector of a plane-wave fluctuation. For spacecraft measurements of solar wind turbulence, the Doppler-shift term typically dominates because the relative velocity of the spacecraft is much larger than the Alfvén velocity, so the Taylor hypothesis [47] is often adopted to convert the frequency spectrum to a wave number spectrum (projected along the sampling direction). The TRICE-2 measurements are in the opposite limit $v_r \ll v_A$, with $v_r = 2.0$ km/s and $v_A = 15\,000$ km/s, potentially enabling us to determine

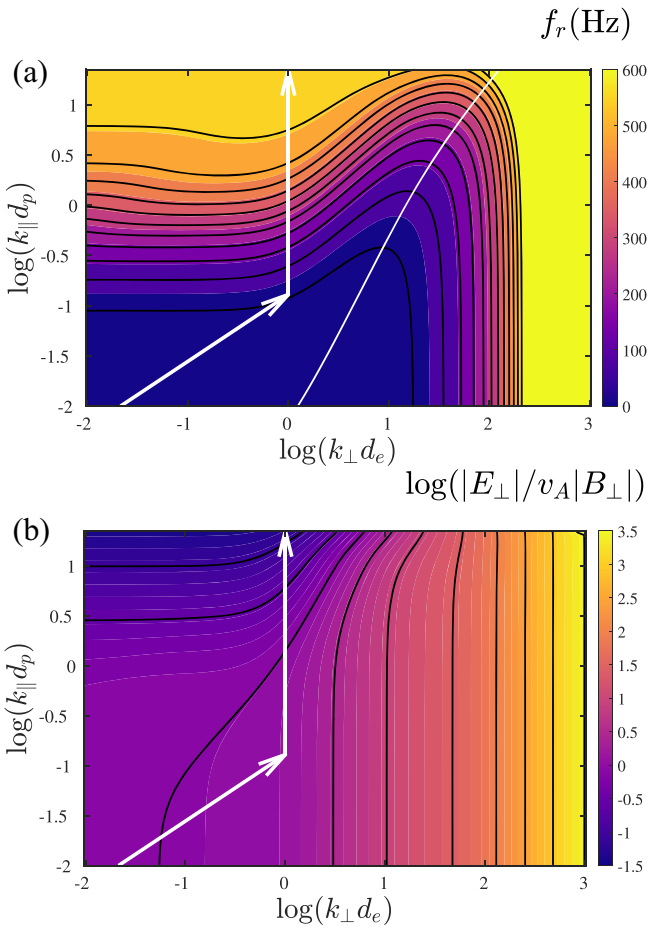

FIG. 4. (a) The estimated rocket-frame frequency f_r for inertial Alfvén waves over the plane $(k_\perp d_e, k_\parallel d_p)$, where the white contour indicates equal plasma-frame frequency and Doppler-shifted contributions, and black contour lines indicate 50 km/s intervals. (b) A plot of the normalized ratio $E_\perp/(v_A B_\perp)$ for the inertial Alfvén wave. The white arrows indicate the direction of the turbulent energy cascade through wave vector space deduced from the turbulent electric and magnetic frequency spectra and the inertial Alfvén wave properties in (a) and (b).

directly the plasma-frame frequency ω. We calculate the linear rocket-frame frequency using $f_r = \omega_r/2\pi \simeq f + k_\perp d_e (v_r/d_e)\sin\theta_{Bv}/2\pi$ (simplified assuming $k_\parallel \ll k_\perp$, to be confirmed *a posteriori*) over the $(k_\perp, k_\parallel)$ plane using the measured rocket velocity and PLUME solutions of the linear inertial Alfvén wave dispersion relation, as shown in Fig. 4(a). Here, the plasma-frame frequency f dominates to the left of the white contour and the Doppler-shift term dominates to the right, indicating that for $k_\perp d_e < 1$ the turbulent energy spectrum measured by TRICE-2 is a true frequency spectrum, rather than the usual interpretation as a Doppler-shifted wave number spectrum.

We can now estimate the perpendicular and parallel wave numbers associated with the spectral break $f = f_{b1}$. Because $E_\perp/(v_A B_\perp) \sim 1$ at $f < f_{b1}$, we interpret the first break f_{b1} as due to the end of the MHD turbulent inertial

range [48] at the transition $k_\perp d_e \sim 1$, corresponding to a perpendicular wavelength $\lambda_\perp = 0.63$ km. Taking $k_\perp d_e \sim 1$ and $k_\parallel d_p \ll 1$, we solve (1) for the parallel wavelength to obtain $\lambda_\parallel = v_A/(f_{b1}\sqrt{2}) = 210$ km. Together, these values yield a wave vector anisotropy at the first break $f_{b1} \simeq 50$ Hz of the turbulent cascade of $k_\parallel/k_\perp \sim 3 \times 10^{-3}$ (confirming our earlier assumption), consistent with the anisotropic cascade typically found at the end of the inertial range in the turbulent solar wind [49]. We also confirm $k_\parallel d_p \ll 1$ using the measured $d_p = 4.3$ km to yield $k_\parallel d_p \sim 0.1$. Note that because the TRICE-2 measurements provide direct measurements of the frequency spectrum in the plasma rest frame at $k_\perp d_e < 1$, we can actually estimate $k_\parallel$ directly from observations, which is not generally possible for a wave number spectrum (determined using Taylor hypothesis) in the usual case of an anisotropic cascade with $k_\perp \gg k_\parallel$.

These results enable us to locate the path of the turbulent energy cascade on the $(k_\perp d_e, k_\parallel d_p)$ plane. In the MHD limit $k_\perp d_e < 1$, the scale-dependent anisotropy of the cascade given by modern theories of MHD turbulence [33,50] scales as $k_\parallel \propto k_\perp^{2/(3+\alpha)}$, with $\alpha = 0$ for the GS95 scaling [33] and $\alpha = 1$ for the B06 scaling [50]. The lower white arrow in Fig. 4 follows the GS95 scaling with an endpoint at $(k_\perp d_e, k_\parallel d_p) = (1, 0.1)$, corresponding to the first break in the energy spectra at $f_{b1} \simeq 50$ Hz. Note that the normalized Poynting flux calculated for the turbulent fluctuations is near zero (not shown), suggesting a balanced cascade of upward and downward propagating Alfvén waves, required for the application of the GS95 or B06 scalings.

Next, we use the observed energy spectra in Fig. 1 and the properties of the inertial Alfvén wave over the $(k_\perp d_e, k_\parallel d_p)$ plane to estimate the path of the turbulent energy cascade through wave vector space beyond the point $(k_\perp d_e, k_\parallel d_p) \sim (1, 0.1)$, corresponding to the frequency range 50 Hz $< f <$ 500 Hz. We use PLUME solutions for the inertial Alfvén wave to plot the normalized ratio $E_\perp/(v_A B_\perp)$ in Fig. 4(b), showing that a decreasing ratio occurs *only* for a cascade to higher $k_\parallel d_p$ values. The observed decrease in the $E_\perp/(v_A B_\perp)$ ratio from the frequency spectra in Fig. 1 is inconsistent with a cascade to $k_\perp d_e > 1$. The only path consistent with both a decrease in $E_\perp/v_A B_\perp$ and an increase in the rocket-frame frequency to $f = f_{b2} = 500$ Hz is a path moving vertically to higher $k_\parallel d_p$, indicated on Fig. 4 as the upper white arrow.

With the knowledge of the path of the turbulent energy cascade through $(k_\perp d_e, k_\parallel d_p)$ plane, we can predict the mechanisms responsible for the dissipation of the turbulent cascade at the second break $f_{b2} = 500$ Hz. Using PLUME solutions of the Vlasov-Maxwell dispersion relation, we can compute the normalized total collisionless damping rate $-\gamma/\omega$ of the inertial Alfvén wave over the $(k_\perp d_e, k_\parallel d_p)$ plane, shown in Fig. 5 (color map and black contours). We can also separate the contributions from the $n = 1$ proton cyclotron damping (green dashed contours) and from electron Landau damping (cyan dashed contours), the two mechanisms found numerically to dominate the total collisionless damping for the parameters of the TRICE-2 observations. This plot suggests that collisionless damping should become significant at $k_\parallel d_p \gtrsim 10$, which corresponds to a rocket-frame frequency of $f_r \gtrsim 500$ Hz [see Fig. 4(a)]. Furthermore, the damping is likely to be a combination of proton cyclotron damping (since $\omega/\Omega_p \to 1$ as $k_\parallel d_p \to 10$) and electron Landau damping (since $\omega/(k_\parallel v_{te}) \to 1$).

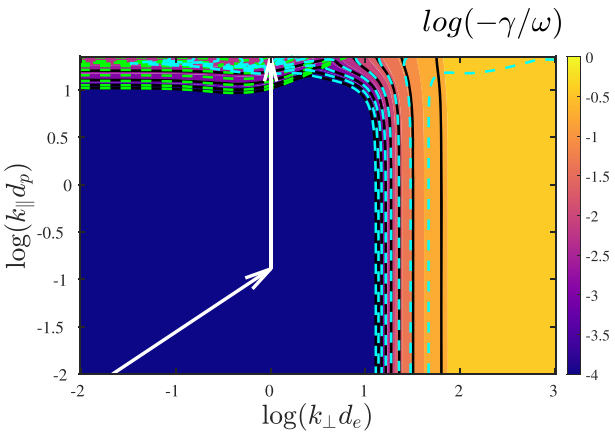

FIG. 5. Plot of the normalized total collisionless damping rate $-\gamma/\omega$ of the inertial Alfvén wave over the $(k_\perp d_e, k_\parallel d_p)$ plane, along with contours for the contributions from the $n = 1$ ion cyclotron damping (green dashed contours) and electron Landau damping (cyan dashed contours).

Conclusions—Here, we observe a new regime of inertial Alfvén wave turbulence in the auroral ionosphere with properties distinct from the typical turbulence observed in the solar wind and other heliospheric plasmas. Ionospheric plasmas may consist of multiple ion species, but a comparison of the electric and magnetic field spectra at low frequencies $f < 50$ Hz implies that, at this altitude $z \sim 1000$ km, the plasma is dominated by protons with an inferred number density ratio $n_O/n_p < m_p/m_O = 1/16$. The low rocket velocity relative to the Alfvén velocity $v_r \ll v_A$, along with the presence of collisionless damping at perpendicular wavelengths smaller than the plasma skin depth, together imply that the measurements represent a frequency spectrum of turbulence, not a Doppler-shifted wave number spectrum, enabling the parallel wave number of the turbulent fluctuations to be estimated directly. The first break in the spectrum at $f_{b1} \sim 50$ Hz is interpreted to be the end of the MHD inertial range, where the turbulent cascade reaches the perpendicular kinetic scale of the electron skin depth $k_\perp d_e \sim 1$. Combining estimates of the rocket-frame frequency and the ratio of the perpendicular electric to the perpendicular magnetic field spectra over the $(k_\perp d_e, k_\parallel d_p)$ plane enables the path of the

turbulent energy cascade over that plane to be determined; we deduce that upon reaching the end of the turbulent MHD inertial range at $k_\perp d_e \sim 1$, the turbulence transitions to a parallel cascade, leading to an increase in $k_\parallel d_p$, corresponding in frequency to $\omega/\Omega_p \to 1$. The second break in the spectrum at $f_{b2} \sim 500$ Hz is interpreted to be the point at which the collisionless damping becomes significant, where the properties of the linear Vlasov-Maxwell dispersion relation for inertial Alfvén waves suggest that the damping is a combination of proton cyclotron damping and electron Landau damping at rocket-frame frequencies $f_r \gtrsim f_{b2}$.

Acknowledgments—We wish to acknowledge the support of the TRICE-2 rocket team. F. D. M. was supported by the Research Council of Norway (RCN) Overseas Research Grant No. ES658406/312055 and G. G. H. was supported by NASA Grant No. 80NSSC18K0643.

[1] K. Stasiewicz, Y. Khotyaintsev, M. Berthomier, and J.-E. Wahlund, Identification of widespread turbulence of dispersive alfvén waves, Geophys. Res. Lett. **27**, 173 (2000).
[2] A. Hasegawa, Particle acceleration by MHD surface wave and formation of aurora, J. Geophys. Res. **81**, 5083 (1976).
[3] C. K. Goertz and R. W. Boswell, Magnetosphere-ionosphere coupling, J. Geophys. Res. **84**, 7239 (1979).
[4] M. C. Kelley, D. J. Knudsen, and J. F. Vickrey, Poynting flux measurements on a satellite: A diagnostic tool for space research, J. Geophys. Res. **96**, 201 (1991).
[5] T. E. Eastman, E. W. Hones Jr., S. J. Bame, and J. R. Asbridge, The magnetospheric boundary layer: Site of plasma, momentum and energy transfer from the magnetosheath into the magnetosphere, Geophys. Res. Lett. **3**, 685 (1976).
[6] C. F. Kennel, Consequences of a magnetospheric plasma, Rev. Geophys. Space Phys. **7**, 379 (1969).
[7] S. Knight, Parallel electric fields, Planet. Space Sci. **21**, 741 (1973).
[8] T. Iijima and T. A. Potemra, Field-aligned currents in the dayside cusp observed by triad, J. Geophys. Res. **81**, 5971 (1976).
[9] K. Stasiewicz, P. Bellan, C. Chaston, C. Kletzing, R. Lysak, and J. Maggs *et al.*, Small scale Alfénic structure in the aurora, Space Sci. Rev. **92**, 423 (2000).
[10] R. L. Lysak and W. Lotko, On the kinetic dispersion relation for shear Alfvén waves, J. Geophys. Res. **101**, 5085 (1996).
[11] C. A. Kletzing, Electron acceleration by kinetic Alfvén waves, J. Geophys. Res. **99**, 11095 (1994).
[12] C. A. Kletzing and S. Hu, Alfvén wave generated electron time dispersion, Geophys. Res. Lett. **28**, 693 (2001).
[13] C. C. Chaston, J. W. Bonnell, C. W. Carlson, J. P. McFadden, R. E. Ergun, and R. J. Strangeway, Properties of small-scale Alfvén waves and accelerated electrons from FAST, J. Geophys. Res. **108**, 8003 (2003).
[14] A. Keiling, J. R. Wygant, C. A. Cattell, F. S. Mozer, and C. T. Russell, The global morphology of wave poynting flux: Powering the aurora, Science **299**, 383 (2003).
[15] C. C. Chaston, C. W. Carlson, J. P. McFadden, R. E. Ergun, and R. J. Strangeway, How important are dispersive Alfvén waves for auroral particle acceleration?, Geophys. Res. Lett. **34**, L07101 (2007).
[16] A. Keiling, S. Thaller, J. Wygant, and J. Dombeck, Assessing the global Alfvén wave power flow into and out of the auroral acceleration region during geomagnetic storms, Sci. Adv. **5**, eaav8411 (2019).
[17] A. Keiling, S. Thaller, J. Dombeck, and J. Wygant, Temporal evolution of substorm-driven global Alfvén wave power above the auroral acceleration region, J. Geophys. Res. **125**, e27444 (2020).
[18] J. W. R. Schroeder, F. Skiff, C. A. Kletzing, G. G. Howes, T. A. Carter, and S. Dorfman, Direct measurement of electron sloshing of an inertial Alfvén wave, Geophys. Res. Lett. **43**, 4701 (2016).
[19] J. W. R. Schroeder, F. Skiff, G. G. Howes, C. A. Kletzing, T. A. Carter, and S. Dorfman, Linear theory and measurements of electron oscillations in an inertial Alfvén wave, Phys. Plasmas **24**, 032902 (2017).
[20] J. W. R. Schroeder, G. G. Howes, C. A. Kletzing, F. Skiff, T. A. Carter, S. Vincena, and S. Dorman, Laboratory measurements of the physics of auroral electron acceleration by Alfvén waves, Nat. Commun. **12**, 3103 (2021).
[21] C. Kletzing, S. A. Fuselier, J. W. Bonnell, J. W. Labelle, J. Moen, K. J. Trattner, and P. M. Steven, The twin rockets to investigate cusp electrodynamics 2 (TRICE-2) mission, *AGU Fall Meeting Abstracts* (2019), Vol. 2019, https://ui.adsabs.harvard.edu/abs/2019AGUFMSM34A..03K/abstract.
[22] C. Moser, J. LaBelle, R. Roglans, J. W. Bonnell, I. H. Cairns, and C. Feltman, C. A. Kletzing, S. Bounds, R. P. Sawyer, and S. A. Fuselier, Modulated upper- hybrid waves coincident with lower- hybrid waves in the cusp, J. Geophys. Res. **126**, e2021JA029590 (2021).
[23] R. P. Sawyer, S. A. Fuselier, C. A. Kletzing, J. W. Bonnell, R. Roglans, and S. R. Bounds *et al.*, TRICE 2 observations of low-energy magnetospheric ions within the cusp, J. Geophys. Res. **126**, e2021JA029382 (2021).
[24] G. Wannberg, I. Wolf, L. G. Vanhainen, K. Koskenniemi, J. RöTtger, M. Postila, J. Markkanen, R. Jacobsen, A. Stenberg, R. Larsen, S. Eliassen, S. Heck, and A. Huuskonen, The EISCAT svalbard radar: A case study in modern incoherent scatter radar system design, Radio Sci. **32**, 2283 (1997).
[25] G. G. Howes, K. G. Klein, and J. M. TenBarge, Validity of the Taylor hypothesis for linear kinetic waves in the weakly collisional solar wind, Astrophys. J. **789**, 106 (2014).
[26] C. H. K. Chen, S. D. Bale, C. Salem, and F. S. Mozer, Frame dependence of the electric field spectrum of solar wind turbulence, Astrophys. J. **737**, L41 (2011).
[27] S. D. Bale, P. J. Kellogg, F. S. Mozer, T. S. Horbury, and H. Reme, Measurement of the electric fluctuation spectrum of magnetohydrodynamic turbulence, Phys. Rev. Lett. **94**, 215002 (2005).

[28] G. G. Howes, W. Dorland, S. C. Cowley, G. W. Hammett, E. Quataert, A. A. Schekochihin, and T. Tatsuno, Kinetic simulations of magnetized turbulence in astrophysical plasmas, Phys. Rev. Lett. **100**, 065004 (2008).
[29] G. G. Howes, J. M. TenBarge, W. Dorland, E. Quataert, A. A. Schekochihin, R. Numata, and T. Tatsuno, Gyrokinetic simulations of solar wind turbulence from ion to electron scales, Phys. Rev. Lett. **107**, 035004 (2011).
[30] G. G. Howes, J. M. Tenbarge, and W. Dorland, A weakened cascade model for turbulence in astrophysical plasmas, Phys. Plasmas **18**, 102305 (2011).
[31] D. Told, F. Jenko, J. M. TenBarge, G. G. Howes, and G. W. Hammett, Multiscale nature of the dissipation range in gyrokinetic simulations of Alfvénic turbulence, Phys. Rev. Lett. **115**, 025003 (2015).
[32] D. Grošelj, A. Mallet, N. F. Loureiro, and F. Jenko, Fully kinetic simulation of 3D kinetic Alfvén turbulence, Phys. Rev. Lett. **120**, 105101 (2018).
[33] P. Goldreich and S. Sridhar, Toward a theory of interstellar turbulence II. Strong Alfvénic turbulence, Astrophys. J. **438**, 763 (1995).
[34] G. G. Howes, S. C. Cowley, W. Dorland, G. W. Hammett, E. Quataert, and A. A. Schekochihin, A model of turbulence in magnetized plasmas: Implications for the dissipation range in the solar wind, J. Geophys. Res. **113**, A05103 (2008).
[35] A. A. Schekochihin, S. C. Cowley, W. Dorland, G. W. Hammett, G. G. Howes, E. Quataert, and T. Tatsuno, Astrophysical gyrokinetics: Kinetic and fluid turbulent cascades in magnetized weakly collisional plasmas, Astrophys. J. Suppl. Ser. **182**, 310 (2009).
[36] C. S. Salem, G. G. Howes, D. Sundkvist, S. D. Bale, C. C. Chaston, C. H. K. Chen, and F. S. Mozer, Identification of kinetic Alfvén wave turbulence in the solar wind, Astrophys. J. Lett. **745**, L9 (2012).
[37] S. Boldyrev, K. Horaites, Q. Xia, and J. C. Perez, Toward a theory of astrophysical plasma turbulence at subproton scales, Astrophys. J. **777**, 41 (2013).
[38] D. Grošelj, C. H. K. Chen, A. Mallet, R. Samtaney, K. Schneider, and F. Jenko, Kinetic turbulence in astrophysical plasmas: Waves and/or structures?, Phys. Rev. X **9**, 031037 (2019).
[39] C. A. Kletzing, D. J. Thuecks, F. Skiff, S. R. Bounds, and S. Vincena, Measurements of inertial limit Alfvén wave dispersion for finite perpendicular wave number, Phys. Rev. Lett. **104**, 095001 (2010).
[40] K. G. Klein and G. G. Howes, Predicted impacts of proton temperature anisotropy on solar wind turbulence, Phys. Plasmas **22**, 032903 (2015).
[41] S. Oughton, E. R. Priest, and W. H. Matthaeus, The influence of a mean magnetic field on three-dimensional magnetohydrodynamic turbulence, J. Fluid Mech. **280**, 95 (1994).
[42] C. S. Ng and A. Bhattacharjee, Interaction of Shear-Alfven wave packets: Implication for weak magnetohydrodynamic turbulence in astrophysical plasmas, Astrophys. J. **465**, 845 (1996).
[43] S. Galtier, S. V. Nazarenko, A. C. Newell, and A. Pouquet, A weak turbulence theory for incompressible magnetohydrodynamics, J. Plasma Phys. **63**, 447 (2000).
[44] J. Cho and E. T. Vishniac, The anisotropy of magnetohydrodynamic Alfvénic turbulence, Astrophys. J. **539**, 273 (2000).
[45] G. G. Howes and K. D. Nielson, Alfvén wave collisions, the fundamental building block of plasma turbulence. I. Asymptotic solution, Phys. Plasmas **20**, 072302 (2013).
[46] C. Y. Johnson, Ion and neutral composition of the ionosphere, Ann. IQSY **5**, 197 (1969).
[47] G. I. Taylor, The spectrum of turbulence, Proc. R. Soc. A **164**, 476 (1938).
[48] G. G. Howes, *Magnetic Fields in Diffuse Media* (Springer, Heidelberg, 2015), Chap. Kinetic Turbulence.
[49] F. Sahraoui, M. L. Goldstein, G. Belmont, P. Canu, and L. Rezeau, Three dimensional anisotropic k spectra of turbulence at subproton scales in the solar wind, Phys. Rev. Lett. **105**, 131101 (2010).
[50] S. Boldyrev, Spectrum of magnetohydrodynamic turbulence, Phys. Rev. Lett. **96**, 115002 (2006).